Impact of subgrid-scale radiative heating variability on the stratocumulus to trade cumulus transition in climate models

Heng Xiao, William I. Gustafson Jr., and Hailong Wang
Atmospheric Sciences and Global Change Division
Pacific Northwest National Laboratory

Initial submission: 26 September 2013

Revision: 17 March 2014

Accepted Article

This article has been accepted for publication and undergone full peer review but has not been through the copyediting, typesetting, pagination and proofreading process which may lead to differences between this version and the Version of Record. Please cite this article as doi: 10.1002/2013JD020999

©2014 American Geophysical Union. All rights reserved.

Abstract

Subgrid-scale interactions between turbulence and radiation are potentially important for accurately simulating marine low clouds in climate models. To better understand the impact of these interactions, the Weather Research and Forecasting (WRF) model is configured for large eddy simulation (LES) to study the stratocumulus-to-trade cumulus (Sc-to-Cu) transition. Using the GEWEX Atmospheric System Studies (GASS) composite Lagrangian transition case and the Atlantic Trade Wind Experiment (ATEX) case, it is shown that the lack of subgrid-scale turbulence-radiation interaction, as is the case in current generation climate models, accelerates the Sc-to-Cu transition. Our analysis suggests that subgrid-scale turbulence-radiation interactions in cloud-topped boundary layers contribute to stronger production of temperature variance, which in turn leads to stronger buoyancy production of turbulent kinetic energy and helps to maintain the Sc cover.

Accepted Article

©2014 American Geophysical Union. All rights reserved.

1. Introduction and motivation

The evolution of marine low clouds as they advect along the trade wind tracks from cold sea surfaces in the subtropical eastern ocean basins to warm surfaces in the tropical western basins, usually known as the "stratocumulus to trade cumulus transition" (the Sc-to-Cu transition) [e.g., Wyant et al., 1997; Bretherton and Wyant, 1997], involves significant changes in the horizontal and vertical structure of the clouds. Most current-generation climate models, both global climate models (GCMs) with grid spacings of ~100 km horizontally, and regional climate models with grid sizes in the 10's of km, are too coarse to fully characterize marine low cloud structures and require parameterizations for subgrid-scale turbulent, microphysical and radiative processes. Due to deficiencies in these parameterizations, it is common to find climate models that either produce insufficient cloud cover near the coast in the subtropical eastern oceans or produce an unrealistic transition from stratocumulus to cumulus away from the coast in terms of cloud cover, thickness, or height [e.g., Wyant et al., 2010]. These low cloud biases contribute significantly towards uncertainties in climate projections [e.g., Soden and Vecchi, 2011].

A common flaw of physical parameterizations in current generation climate models is that they lack the representation of *subgrid-scale* interactions among different processes, e.g., radiation, microphysics and turbulence, because most parameterizations are designed as modules that only interact with dynamics and other parameterizations on the *grid-scale* [e.g., Randall et al., 2003; Cole et al., 2005]. For example, the turbulence parameterization only sees the grid-cell mean temperature and radiative heating. The adequacy of only predicting the grid-cell means while neglecting the subgrid-scale variability of radiative heating is questioned by Cole et al. [2005]. It is well known that accurate calculation of the mean radiative heating in a climate model grid box is not a simple task [e.g., Pincus et al. 2003, Calahan et al. 1994], and correctly representing the subgrid variability is even harder. However, climate modelers and parameterization developers realize more and more the need for parameterizing subgrid-scale interactions among different processes, especially in light of new findings from detailed process studies. As an example of subgrid-scale interaction between microphysics and turbulence, it has been shown with field campaign in-situ observations and large eddy simulations (LES) that in precipitating stratocumuli evaporation of drizzle in the subcloud layer can drive (1) cloud-scale circulations that enhance updrafts, leading to the formation of open-cell structures; and (2) mesoscale circulations that transport moisture and aerosol between regions with different drizzle intensity [Wood et al., 2011;

©2014 American Geophysical Union. All rights reserved.

Wang and Feingold, 2009a, 2009b; Feingold et al., 2010]. We note that the neglect of such subgrid-scale interaction between microphysics and turbulence could lead to climate model biases in addition to those associated with the neglect of subgrid-scale variability in the formulations of various microphysical processes within a given microphysics parameterization. The latter kind of bias has been pointed out by, among others, Larson et al. [2001] and Pincus and Klein [2000].

In this study, we focus on the possible impact of subgrid-scale interactions between radiation and turbulence on the Sc-to-Cu transition in the marine boundary layer (MBL). We are motivated by two arguments: (1) climatologically speaking, if one tracks an air column in the MBL from an overcast stratocumulus condition to a broken shallow cumulus condition, they would find that the stratocumulus cover stays significant (i.e., higher than typical shallow cumulus cloud fraction of 0.1-0.2) for a considerable part of its journey, and cloud-top radiative cooling is important for maintaining turbulent mixing in the cloud layer [e.g., Xiao et al., 2011; Lewellen and Lewellen, 2002]; and (2) along its Lagrangian track a stratocumulus-topped MBL usually gets more and more horizontally inhomogeneous [e.g., Wood and Hartmann, 2006]. It also becomes decoupled vertically [e.g., Wyant et al., 1997].

In previous LES and cloud resolving model studies it has been demonstrated that spatially averaging the radiative heating rates, or doing radiation calculations at longer time intervals than the time step for dynamics and/or other physical parameterizations—equivalent to spatial averaging in doubly-periodic domains—could lead to bias growth in deep convection regimes [e.g., Xu and Randall, 1995]. Such temporal or spatial smoothing decreases the horizontal variability of radiative heating seen by other parts of the model, thus reducing the interactions between turbulence and radiation on scales smaller than the averaging scale.

By using a spatial averaging technique in an LES, we aim to examine the impact of turbulence-radiation interactions on scales unresolved in GCMs in the context of the Sc-to-Cu transition.

2. The model and experiment design

We use the Advanced Research Weather Research and Forecasting (WRF) model (ARW) v3.3.1 configured for LES [Skamarock et al., 2008; Wang et al., 2009; Yamaguchi and Feingold, 2012]. We analyze simulations from the composite transition case (http://www.mpimet.mpg.de/en/mitarbeiter/irina-sandu/transition-cases.html, the reference

©2014 American Geophysical Union. All rights reserved.

Accepted Article

setup is used.) and the Atlantic Trade Wind Experiment (ATEX) case [Stevens et al., 2001] in the GEWEX Atmospheric System Studies (GASS) Boundary Layer Clouds Working Group inter-comparison projects.

The composite transition case is an idealized Lagrangian case for the Sc-to-Cu transition based on the observational study of the transitions in boundary layer cloudiness in the eastern subtropical oceans described in Sandu et al. [2010]. The initial condition, boundary conditions, and external forcing are supplied for a "typical" lower troposphere air column starting in the subtropical Northeastern Pacific (25°N, 125°W) that moves southwestward along the trade wind track. The simulation starts at 10 a.m. local time on 15 July and lasts for 72 hours. The initial condition is a well-mixed MBL capped by an inversion with an ~11 K temperature jump at ~900 m. Sea surface temperature (SST) increases from 20.6°C to 26.0°C while horizontal large-scale divergence is constant (1.86×10^{-6} s^{-1}) in time. In the vertical, horizontal divergence is constant from the surface to 2000 m; from 2000 m to the model top (3000 m) subsidence itself is kept constant at $2000\times1.86\times10^{-6}$ m s^{-1}. To have a domain representative of a GCM grid box, we use a domain with 192×192 grid points and a horizontal grid spacing of 300 m, resulting in a 57.6×57.6 km^2 domain. The vertical grid spacing is ~30 m with 100 levels. For this case we use the CAM3 radiation [Collins et al., 2006] and WDM6 microphysics [Lim and Hong, 2010] parameterizations in WRF. The sensitivity to model resolution and radiation parameterization for this case is discussed in Sec. 3.2.

The ATEX case is a quasi-steady case based on observations of trade-wind cumuli under a strong inversion. This case has substantial cloud cover (so cloud top radiative cooling is important) but greater spatial inhomogeneity than a typical well-mixed Sc-topped MBL case. It has been studied as a typical "cumulus-under-stratus" regime, an important phase during the Sc-to-Cu transition [Lock, 2009; Xiao et al., 2011]. We follow Stevens et al. [2001] in our setup. The simulation is 18 hours long with only longwave radiation (nighttime condition) and we analyze results after the first 8 hours, when the cloud layer evolution becomes approximately quasi-stationary. The horizontal grid spacing is 150×150 m^2 and vertical grid spacing is ~30 m. The domain has 128×128 grid points in the horizontal and 100 levels in the vertical. This domain (19.2×19.2 km^2) is smaller than the composite transition case and more comparable to a contemporary regional climate model grid box. For this case we use the WDM6 microphysics as in the composite transition case, and we run two sets of

©2014 American Geophysical Union. All rights reserved.

simulations to compare the impact of the radiation scheme selection, one with the CAM3 radiation and the other with the RRTMG radiation [Iacono et al. 2008].

In addition to the control simulations, we perform sensitivity experiments in which the horizontal inhomogeneity in radiative heating rates is removed. As shown schematically in Fig. 1, instead of passing the actual radiative heating rate (Q_R) at each grid point to the temperature prediction equation in the dynamics, we pass the horizontally averaged radiative heating rate ($\overline{Q_R}$), thus removing the horizontal anomalies ($Q_R{}'$) in the radiative heating rate seen by the dynamic equations. If we think of the LES as a Single Column Model (SCM) with almost perfect parameterizations for microphysics, radiation and boundary layer turbulence and the interactions among them, then this horizontal averaging procedure artificially prevents the "turbulence parameterization" (i.e., dynamics mostly resolved in a LES but parameterized in a SCM) from interacting with radiation on scales smaller than the LES domain size. In other words, our experiment design mimics what happens in a real GCM or SCM where subgrid-scale radiation-turbulence interactions are currently not considered. By comparing these experiments with the control simulations, we can assess the impact of subgrid-scale turbulence-radiation interaction in a typical climate model on the simulated Sc-to-Cu transition. Similar techniques have been used in the study of cloud-radiation feedback in deep convection [e.g., Xu and Randall 1995; Bretherton et al. 2005].

3. The impact of radiative heating horizontal variability

3.1 The composite transition case

First, we present the effects of horizontal radiative heating variability in the composite transition case. In this case, we turn on horizontal averaging of radiative heating six hours after the simulation starts so that the turbulence structure in the boundary layer gets established before removing horizontal radiative heating variability. Figure 2a-c shows the evolution of domain averaged total cloud fraction, liquid water path (LWP), and inversion height (defined as the level of maximum total water mixing ratio gradient) for the control and the experiment. For the control, we see (1) breakup of clouds during the day and recovery at night, and (2) a decreasing trend in cloud cover and LWP while the inversion height grows from ~950 to 1780 m. These features are in good agreement with preliminary results from the composite transition inter-comparison project (available from the model inter-comparison website of the Boundary Layer Cloud Working Group (BLCWG) of the GEWEX Cloud System Studies (GCSS) at http://www.knmi.nl/samenw/rico/RICO/). The mean cloud cover

©2014 American Geophysical Union. All rights reserved.

in the horizontal-averaging experiment is 20-40% lower than in the control from the second day on; the decrease in mean LWP is also significant (the peak value is reduced by 40 g m^{-2} in the first day); the inversion height at the end of the simulation is about 200 m lower than in the control. The difference in the vertical distribution of mean cloud cover between the control and the experiment, shown in Fig. 2d, is consistent with the differences in total cloud fraction and LWP. Note that the vertical coordinate in Fig. 2d is the height above sea level normalized by the domain averaged inversion height. During the first 2-3 hours of averaging, we see a small increase (5–10%) in cloud cover in the upper cloud layer but very soon a large decrease appears in the lower portion of the cloud. As time goes on, the negative response prevails in the stratus portion of the cloud layer (enclosed by the 5% cloud fraction contour) and a slight increase (less than 5%) in cloud fraction appears near cloud base from the middle of the second day on. The surface precipitation is negligible in both the control and the experiment.

Figure 3 shows domain averaged total water, liquid water, buoyancy production of TKE (resolved), and radiative heating rate ($\overline{Q_R}$) and its horizontal standard deviation at three different times after horizontal averaging is applied. The upper row shows hourly averages during the first hour of horizontal averaging. There is a very slight increase (barely visible) in the mean liquid water mixing ratio (Fig. 3b) and radiative cooling rate (Fig. 3d) in the upper part of the cloud layer, consistent with the increase in cloud cover seen in Fig. 2d. The reason for this increase is discussed in more detail in connection with the ATEX case in the following subsection. In contrast to this slight increase in the mean cloud top radiative cooling, there is a sizable decrease (5-10%) in buoyancy production of TKE in the domain (Fig. 3c). Since mean radiative cooling near cloud top actually increases, this decrease has to be explained by the removal (averaging out) of horizontal variability in radiative cooling (see the standard deviation of radiative heating rates in Fig. 3d), which contributes nontrivially to buoyancy production in the domain. Six hours later (the middle row), we see clear decreases in mean cloud water amount (Fig. 3f), cloud top radiative cooling and cloud layer buoyancy production. There is also a change in the vertical structure of mean total water mixing ratio: the MBL is less well-mixed in the averaging experiment with increased total water in the subcloud layer and a decrease in the cloud layer (Fig. 3e). This increase in the subcloud layer moisture leads to a lower cloud base later in the simulation. These changes in the mean state indicate that the impact of the averaging procedure has been amplified by feedbacks through the mean state. A day later (the bottom row), we see in the averaging experiment (1) lowering

©2014 American Geophysical Union. All rights reserved.

of cloud top by ~100 m (Figs. 3i-j); (2) less liquid water in the upper cloud layer but a slight increase near cloud base (Fig. 3j, ~700 m, see also Fig. 2d); and (3) more significant decoupling between the cloud and subcloud layers in terms of total water mixing ratio. Here, stronger decoupling, shallower cloud top (implying weaker cloud top entrainment), and more cumulus-like cloud structure can all be explained by a reduction in the buoyancy production in the cloud layer, which can be traced back to the first hour of averaging. The results shown in Figs. 2 and 3 suggest that removing the horizontal variability in the radiative heating accelerates the Sc-to-Cu transition. In other words, radiative heating horizontal inhomogeneity contributes to maintaining the Sc layer during the transition.

At the surface, due to decreased cloud cover in the averaging experiment, there is an increase in the net shortwave radiation flux into the ocean of ~25 W m^{-2} averaged over the 3-day period. This implies that ignoring the effect of radiative heating horizontal variability on turbulent mixing in cloud-topped MBLs could potentially contribute to SST biases in regions with significant marine low cloud cover in coupled climate models.

3.2 Sensitivity experiments for the composite transition case

(1) Doubling the radiative heating horizontal variability

In the first sensitivity test, instead of replacing Q_R with $\overline{Q_R}$ in the temperature tendency calculation, we replace it with $\overline{Q_R} + 2Q_R{}'$. So instead of removing the horizontal radiative heating anomaly, we double the horizontal variability of radiative heating while keeping the mean the same. Bretherton et al. [2005] used the same technique in their study of deep convective cloud-radiative feedback. The results from this experiment are shown in Fig.4. As expected, doubling the horizontal variability of Q_R has the opposite impact on the Sc-to-Cu transition as removing it: total cloud fraction is always 100%; LWP is significantly larger than that in the control; and, the cloud top reaches higher due to more energetic cloud-top entrainment. Again this proves the point that horizontal inhomogeneity in Q_R contributes to maintaining the Sc layer during the transition.

(2) Sensitivity to resolution

In the second test, we repeat the control and the horizontal-averaging experiment with a higher resolution (100 m in the horizontal and 15 m in the vertical) and a smaller horizontal domain size (19.2×19.2 km^2). The model time step is also reduced from one to half a second. The high-resolution control (Fig. 5) shows similar evolution of cloud fraction, LWP, inversion height and cloud layer structure as the low-resolution control (Fig. 2). But there are

©2014 American Geophysical Union. All rights reserved.

significant quantitative differences. Figure 5b shows that the high-resolution control produces smaller LWP than the low-resolution control (Fig. 2b). This sensitivity of LWP to spatial resolution warrants further investigation into the resolution dependent behavior of WRF LES, especially that of the microphysics schemes. The total cloud fraction in the high-resolution control (Fig. 5a) also shows larger fluctuations in the second and third day, partly due to the reduction in domain size. Despite these differences, the response to the horizontal averaging of radiative heating is very consistent between the low- and high-resolution setups in terms of total cloud fraction, LWP, and inversion height. More importantly, the response in the cloud vertical structure (Fig. 5d) is also very similar except that the increase in cumulus plumes below the Sc layer is slightly more prominent in the high-resolution setup.

In a recent WRF LES study, Yamaguchi and Feingold (2012) found that LWP in their high-resolution stratocumulus simulations converges only with a small physical time step and a large number of acoustic wave sub-steps per physical time step. To test this sensitivity to temporal resolution, we performed shorter (one-day) high-resolution simulations using a smaller time step (0.2 s). We find that the LWP in the control simulation is slightly larger (by about 5 g m^{-2} on average) than that with 0.5 s time step and the response to horizontal averaging also slightly stronger (figures not shown).

To summarize, even though cloud properties such as LWP and cloud fraction in our WRF LES simulations are quantitatively sensitive to the spatial and temporal resolutions, the response to horizontal averaging of radiative heating is very robust.

(3) Sensitivity to the choice of radiation parameterization

In the third test, we repeat the control and the horizontal-averaging experiment using the RRTMG radiation parameterization. As can be seen in Fig. 6, changing the radiation scheme makes relatively small difference in the response to the horizontal averaging of Q_R. One noticeable difference is that with the RRTMG radiation scheme, the inversion height reduction due to the averaging is smaller than that with the CAM radiation scheme. We also see that the daytime breakup of cloud cover is stronger with the RRTMG radiation parameterization than with CAM3, probably because the default treatment of shortwave radiative transfer through the air column above the model top at 3 km is different between the two schemes.

©2014 American Geophysical Union. All rights reserved.

3.3 The ATEX case

In the ATEX case, we focus on the initial transient response to horizontal averaging. Here, we turn on horizontal averaging eight hours after initialization. Figure 7 shows the changes in cloud cover vertical distribution for the two simulations using (a) CAM3 and (b) RRTMG longwave radiation schemes respectively. First, the control simulation with the CAM3 radiation produces slightly more cloud than that with the RRTMG radiation (28 versus 27% in terms of total cloud fraction averaged over the last three hours; These values are smaller than the multi-model ensemble mean but within the bounds of inter-model variability found in Stevens et al. [2001]).

The response to horizontal averaging also has a very similar pattern between the two radiation choices. In the first several hours, a thin layer with increased cloud cover develops near cloud top in the averaging experiment, consistent with what happens in the composite transition case (Fig. 2d). Several hours later this increase in cloud fraction becomes a decrease in the Sc layer. We offer a tentative explanation for this transient behavior based on the temporal evolution of the TKE response to horizontal averaging. As shown in Fig. 8, the initial response in TKE and turbulent mixing to the removal of radiative heating variability is a small decrease restricted to near the cloud top. This leads to local increases in total water mixing ratio (not shown) and cloud amount near cloud top, probably due to reduced mixing with dry air above. The TKE change can be seen to reach deeper in the cloud layer as larger eddies in the cloud layer. Even updrafts/downdrafts reaching into the subcloud layer get affected. Eddy transport of moisture in the cloud layer weakens, masking out the initial increase in cloud water near cloud top. After the first few hours we see increased cumulus activity in the lower part of the cloud layer in Fig. 7, which can be identified by the sporadic pulses of increased cloud cover, similar to Figs. 2d, 5d and 6d.

In another set of simulations of marine stratocumulus with the DYCOMS-II RF01 setup [Stevens et al. 2005], we find that the response to horizontal averaging of radiative heating rate is similar to that in the ATEX case, except the magnitude is relatively small (results not presented here). The stratocumulus layer does not really break up after 10 hours of radiation averaging—total cloud fraction drops from 98.5% to 95% and LWP from 72 to 65 g m^{-2}. This is likely due to the difference in the PBL structure between the DYCOMS-II RF01 case and the other two cases (ATEX and composite transition). The former is a quasi-steady case, typical of the coastal stratocumulus regime with uniform cloud cover and a shallow, well-mixed PBL structure. Turbulent mixing driven by the mean radiative cooling

©2014 American Geophysical Union. All rights reserved.

alone is strong enough to maintain the well-mixed PBL structure in the DYCOMS-II RF01 case, without the contribution from subgrid-scale turbulence–radiation interaction. In the composite transition case the PBL is deeper and already decoupled during the first night (e.g., the negative buoyancy production near cloud base in Fig. 3c) The PBL is also decoupled in the ATEX case. For decoupled PBLs, weakened turbulence–radiation interaction leads to weaker mixing within the cloud layer and between the cloud and subcloud layers (i.e., stronger decoupling, see Fig. 3e), which leads to preferential drying of the Sc deck region at the top (not shown) because less moisture transport can reach it. This forms a feedback loop to break up the Sc deck. In contrast, in the DYCOM-II RF01 case the drying in response to weakened turbulence–radiation interaction is more evenly spread over the upper two thirds of the boundary layer (not shown) due to more efficient vertical mixing. Thus we expect the simulation of the Sc-to-Cu transition to be more sensitive to the details of subgrid-scale turbulence–radiation interaction than that of the well-mixed Sc-topped PBL.

4. Implications for low cloud parameterizations

It is well known that cloud-top radiative cooling is an important process maintaining turbulent mixing in the Sc-topped MBL [e.g., Lilly 1968]. For climate models, the first-order problem is to reproduce the vertical profile of mean radiative heating ($\overline{Q_R}$). But there are important features in the profile of $\overline{Q_R}$ (see, e.g., the solid lines in Fig. 3d) that current-generation climate models have difficulties in representing, e.g., (1) the sharp peak in cloud-top radiative cooling, usually concentrated within a layer of 100 m or less, and (2) residual cooling above the main peak of cloud-top radiative cooling due to horizontal variability of the local cloud top (indicated by the black arrow in Fig. 3d). These difficulties arise in climate models mainly due to coarse vertical resolution and due to the fact that radiation schemes have only the grid-scale mean cloud fields as input. It is currently common practice in climate models to explicitly parameterize the enhancement of buoyancy generation of TKE, or even of cloud-top entrainment directly, due to the difference between the $\overline{Q_R}$ profile in reality (or in LES) and that in climate models [e.g., Bretherton and Park, 2009; Moeng et al., 1999; Randall and Schubert, 2004]. Usually a simple assumption is made in the parameterization that this difference (denoted by $\Delta\overline{Q_R}$) affects the buoyancy flux but not the grid-scale temperature, i.e.,

$$\frac{d\overline{\theta}}{dt} = -\frac{\partial \Delta\overline{w'\theta'}}{\partial z} + \Delta\overline{Q_R} \approx 0, \qquad (1)$$

©2014 American Geophysical Union. All rights reserved.

where θ is potential temperature and w is vertical velocity. $\overline{w'\theta'}$ here can be seen as the buoyancy flux if we ignore the virtual temperature effect for simplicity. $\Delta\overline{Q_R}$ is usually parameterized based on simple models of radiative transfer in cloudy columns [see, e.g., Park and Bretherton, 2009]. Then the equation is solved for $\Delta\overline{w'\theta'}$, which stands for the enhancement of the buoyancy flux due to $\Delta\overline{Q_R}$. The horizontal variability of radiative heating represented by $Q_R{}'$ does not enter the picture at all.

Theoretically speaking, the radiative heating inhomogeneity can affect the buoyancy flux directly as shown in the following tendency equation for the potential temperature eddy flux,

$$\frac{\partial\overline{w'\theta'}}{\partial t} = -\overline{w}\frac{\partial}{\partial z}\overline{w'\theta'} - \overline{w'\theta'}\frac{\partial\overline{w}}{\partial z} - \overline{w'^2}\frac{\partial\overline{\theta}}{\partial z} - \frac{\partial}{\partial z}\overline{w'^2\theta'} + \frac{g}{\overline{\theta_v}}\overline{\theta_v'\theta'} + \frac{1}{\overline{\rho}}\overline{p'\frac{\partial\theta'}{\partial z}} + \overline{Q_R'w'} \ldots , \quad (2)$$

where p is pressure, ρ is air density and θ_v is virtual potential temperature. The assumptions that lead to the general form of Eq. (2) (without the last term) from the original Reynolds Stress equation can be found in books like Stull [1982, Eq. 4.4.3c]. Here we omitted terms due to LES subgrid-scale parameterization and due to molecular diffusion. The last term in Eq. (2) represents the correlation between radiative heating and vertical velocity perturbations [see also Stull, 1982, Eq. 4.4.3a]. For the composite transition case (both high- and low-resolutions), we find that $\overline{Q_R{}'w'}$ is usually two to three orders of magnitude smaller than the other terms on the right-hand side even though its contribution to the budget is positive. Also, when comparing differences for the individual terms on the right-hand side of Eq. (2) between the control and horizontal-averaging experiment we find that the difference for $\overline{Q_R{}'w'}$, which is zero by definition in the horizontal-averaging experiment, is much smaller than the differences for many of the other terms (e.g., $\frac{g}{\overline{\theta_v}}\overline{\theta_v'\theta'}$). So it is more likely that horizontal inhomogeneity in radiative heating impacts buoyancy flux through its effect on other terms in Eq. (2) that involve θ', e.g., $\frac{g}{\overline{\theta_v}}\overline{\theta_v'\theta'}$.

This is in agreement with the work of André et al. [1978], who argued that for the nighttime clear boundary layer the temperature-radiation correlation term, $\overline{\theta' Q_R{}'}$, is of the same order of magnitude as other terms in the tendency equation for potential temperature variance ($\overline{\theta'^2}$) and more important than $\overline{Q_R{}'w'}$. The tendency equation for $\overline{\theta'^2}$ can be written as the following,

©2014 American Geophysical Union. All rights reserved.

$$\frac{\partial\overline{\theta'^2}}{\partial t} = -\overline{w}\frac{\partial\overline{\theta'^2}}{\partial z} - 2\overline{\theta' w'}\frac{\partial\overline{\theta}}{\partial z} - \frac{\partial}{\partial z}\overline{w'\theta'^2} + 2\overline{\theta' Q_R{}'} \ldots, \qquad (3)$$

where dissipation terms due to LES subgrid-scale mixing and due to molecular diffusion are not included. André et al. included a simple parameterization for $\overline{\theta' Q_R{}'}$ in their third-order turbulence closure, where $\overline{\theta' Q_R{}'}$ is assumed to be a pure dissipation term with the form $-0.1\overline{q}\overline{\theta'^2}$ ($\overline{q}$ is the mean water vapor mixing ratio) [see also Coantic and Simonin, 1984]. For the composite transition case, we find that $\overline{\theta' Q_R{}'}$ is also of the same order of magnitude as the other terms in the tendency equation for $\overline{\theta'^2}$ in the high-resolution control (see Fig. 9 for a typical snapshot); but in our case $\overline{\theta' Q_R{}'}$ is *positive*. This is true throughout the simulation, which means for a cloud-topped boundary layer $\overline{\theta' Q_R{}'}$ cannot be treated as a simple damping term (like thermal conduction) for temperature variance. The same conclusion is reached when we use liquid water potential temperature instead of potential temperature for the budget analysis. We think the difference in the sign of $\overline{\theta' Q_R{}'}$ is because under clear conditions positive θ' always leads to stronger longwave radiative cooling (negative $Q_R{}'$ from increased emissions relative to cooler nearby parcels) while for a cloud-topped boundary layer air parcels with positive θ' near the cloud top are likely to be cloud-free due to mixing with warmer and drier free-troposphere air, and thus have weaker longwave cooling (positive $Q_R{}'$) than cloudy parcels. Positive $\overline{\theta' Q_R{}'}$ contributes to the production of $\overline{\theta'^2}$, which in turn leads to stronger buoyancy flux through $\frac{g}{\overline{\theta_v}}\overline{\theta_v'\theta'}$ in Eq. (2).

Potentially the radiative heating perturbation term ($Q_R{}'$) can also affect other second-order moments like the covariance between water vapor mixing ratio and potential temperature $\overline{q_v{}'\theta'}$ or that between liquid water mixing ratio and potential temperature $\overline{q_l{}'\theta'}$, which can eventually affect the buoyancy flux ($\overline{w'\theta_v{}'}$) budget. Our analysis shows that these effects are negligible in the composite transition case.

In summary, the above budget analysis for various second-order moments suggests that the leading-order impact of radiative heating perturbations on turbulence is through its impact on the potential temperature variance. In the clear boundary layer simulation of André et al. [1978], radiation-turbulence interaction damps nighttime turbulent mixing. But in the composite transition case, we find that radiative heating horizontal inhomogeneity promotes turbulent mixing and is important for the maintenance of cloud during the Sc-to-Cu transition. We think it is worthwhile to explore the benefit of parameterizations for $\overline{\theta' Q_R{}'}$ more suitable for cloudy boundary layers than that of André et al. in high-order turbulence

©2014 American Geophysical Union. All rights reserved.

schemes. This is especially true since high-order schemes are now more widely implemented in climate models with the hope to improve the simulation of marine low clouds [e.g., Golaz et al. 2002; Cheng and Xu, 2006]. For lower-order turbulence schemes that do not calculate second-order moments like temperature variance, we may need to parameterize the impact of subgrid-scale turbulence-radiation interaction on buoyancy flux or even directly on TKE.

5. Conclusion

To conclude, we have investigated the impact of horizontal variability of radiative heating in the context of the Sc-to-Cu transition. This was done with large eddy simulations with the WRF model configured for the GASS composite Lagrangian transition case with a large domain (~60×60 km^2) comparable to a GCM grid box. We remove the horizontal variability in radiative heating rates by applying horizontal domain averages at each grid point to assess the impact of neglecting subgrid-scale turbulence-radiation interactions on the simulated Sc-to-Cu transition in climate models. Our results show that cloud cover and LWP are significantly reduced, allowing more shortwave radiation to reach the surface (~25 W m^{-2} on average in the case considered); the inversion height drops by 200 m at the end of the 3-day simulation; and the boundary layer structure also gets much less well-mixed. In short, removing subgrid-scale turbulence-radiation interactions "accelerates" the transition from Sc to shallow Cu. The qualitative pattern and relative magnitude of the response to the horizontal averaging of radiative heating rates are quite robust throughout the experiments we have done, even though there is quantitative dependence of the response on model resolution and the choice of radiation parameterizations. We expect to find similar quantitative dependence on the specific LES model used to conduct the experiments. For the ATEX case we also find a similar response albeit the magnitude of the response is smaller. For a well-mixed Sc-topped PBL like that in the DYCOMS-II RF01 case, even though the structure of the response in the cloud layer is similar to the two cases above, the magnitude of the response is relatively smaller. The Sc deck does not really break up in the DYCOMS-II case, probably because the mean radiative cooling alone is strong enough to maintain the well-mixed PBL structure.

Given the importance of cloud-top radiative cooling in maintaining turbulent mixing in cloud-topped boundary layers, climate models nowadays parameterize the impact of underrepresented vertical structures in the mean radiative heating profile. Our results further suggest that unresolved horizontal structures, i.e., horizontal subgrid-scale variability in radiative heating, can contribute significantly to the maintenance of marine low clouds and

©2014 American Geophysical Union. All rights reserved.

boundary layer turbulence during the Sc-to-Cu transition. We find that, radiative heating perturbations, rather than just damping temperature variance, like in clear boundary layers, actually contribute to the production of temperature variance in the cloudy composite transition case. This in turn contributes to the buoyancy production of TKE. In the third-order turbulence scheme of André et al. [1978] the effect of radiative heating perturbations is parameterized as a simple damping term in the temperature variance equation. We argue that for cloud-topped boundary layers a more complicated parameterization is necessary for high-order turbulence schemes. Lower-order schemes would also benefit if the effect of radiative heating subgrid-scale variability were to be parameterized. We also note that if the effect of three-dimensional radiative transfer were to be considered in the simulations, the impact of the turbulence–radiation interaction is likely to be even stronger than what we have found.

Acknowledgements. Funding for this manuscript has been provided by a U.S. Department of Energy (DOE) Early Career grant awarded to Dr. Gustafson. H. Wang also acknowledges support from the DOE Earth System Modeling Program. The Pacific Northwest National Laboratory Institutional Computing program, and the Environmental Molecular Science Laboratory, a national scientific user facility sponsored by the Department of Energy's Office of Biological and Environmental Research, provided high performance computing resources. The Pacific Northwest National Laboratory is operated for DOE by Battelle Memorial Institute under Contract No. DE-AC05-76RL01830. We gratefully acknowledge our usage of the WRF-LES driver and statistics packages from Dr. Takanobu Yamaguchi, from http://ersl.noaa.gov/csd/staff/tak.yamaguchi/code/. We are also grateful to Drs. Peter Blossey, Stephan de Roode, Robert Pincus, and Larry Berg and to three anonymous reviewers for their very helpful comments on an earlier version of the manuscript.

Accepted Article

©2014 American Geophysical Union. All rights reserved.

References

André, J. C., G. De Moor, P. Lacarrére, G. Therry and R. Du Vachat (1978), Modeling the 24-hour Evolution of the Mean and Turbulent Structures of the Planetary Boundary Layer. *J. Atmos. Sci.*, *35*, 1861–1883, doi: 10.1175/1520-0469(1978)035<1861:MTHEOT>2.0.CO;2.

Bretherton, C. S. and M. C. Wyant (1997), Moisture transport, lower-tropospheric stability, and decoupling of cloud-topped boundary layers. *J. Atmos. Sci.*, *54*, 148–167.

Bretherton, C. S., P. N. Blossey and M. Khairoutdinov (2005), An Energy-Balance Analysis of Deep Convective Self-Aggregation above Uniform SST. *J. Atmos. Sci.*, *62*, 4273–4292.

Bretherton, C. S. and S. Park (2009), A new moist turbulence parameterization in the Community Atmosphere Model. *J. Climate*, 22, 3422–3448.

Cahalan R.F., W. Ridgway, W.J. Wiscombe, T.L. Bell, and J. B. Snider (1994), The albedo of fractal stratocumulus clouds. *J. Atmos. Sci.*, 51, 2434–2455.

Cheng, A. and K.-M. Xu (2006), simulation of shallow cumuli and their transition to deep convective clouds by cloud-resolving models with different third-order turbulence closures. *Quart. J. Roy. Meteor. Soc.*, 132, 359–382.

Coantic, M. and O. Simonin (1984), Radiative effects on Turbulent Temperature Spectra and Budgets in the Planetary Boundary Layer. *J. Atmos. Sci.*, *41*, 2629–2651.

Cole, J. N. S., H. W. Barker, W. O'Hirok, E. E. Clothiaux, M. F. Khairoutdinov, and D. A. Randall (2005), Interactions between Clouds and Radiation at Scales Unresolved by Global Climate Models. *Geophys. Res. Lett.*, *32*, L19817, doi:10.1029/2005GL023329.

Collins, W. D., P. J. Rasch, B. A. Boville, J. J. Hack, J. R. McCaa, D. L. Williamson, B. P. Briegleb, C. M. Bitz, S. J. Lin, and M. H. Zhang (2006), The formulation and atmospheric simulation of the Community Atmosphere Model version 3 (CAM3), *J. Climate*, *19*, 2144–2161.

Feingold G., I. Koren, H. Wang, H. Xue, and W. Brewer (2010), Precipitation-generated oscillations in open cellular cloud fields. *Nature*, *466*, 849–852.

Golaz, J.-C., V. E. Larson, and W. R. Cotton (2002), A PDF-Based Model for Boundary Layer Clouds. Part I: Method and Model Description. *J. Atmos. Sci.*, *59*, 3540–3551.

Larson, V. E., R. Wood, P. R. Field, J.-C. Golaz, T. H. Vonder Haar, W. R. Cotton (2001), Systematic Biases in the Microphysics and Thermodynamics of Numerical Models that Ignore Subgrid Variability. *J. Atmos. Sci.*, 58, 1117–1128.

Iacono, M., J. Delamere, E. Mlawer, M. Shephard, S. Clough, and W. Collins (2008), Radiative forcing by long-lived greenhouse gases: Calculations with the AER radiative transfer models. *J. Geophys. Res.*, *113*, D13103, doi:10.1029/2008JD009944.

Lewellen D. and W. Lewellen (2002), Entrainment and decoupling relations for cloudy boundary layers. *J. Atmos. Sci.*, *59*, 2966–2986.

©2014 American Geophysical Union. All rights reserved.

Accepted Article

Lilly, D., 1968: Models of cloud-topped mixed layers under a strong inversion. *Quart. J. Roy. Meteor. Soc.*, *94*, 292–309.

Lim, K. S. S., and S. Y. Hong (2010), Development of an effective double-moment cloud microphysics scheme with prognostic cloud condensation nuclei (CCN) for weather and climate models, *Mon. Wea. Rev.*, *138*, 1587–1612, doi:10.1175/2009mwr2968.1.

Lock, A. (2009) Factors influencing cloud area at the capping inversion for shallow cumulus clouds. *Quart. J. Roy. Meteor. Soc.*, *135*, 941–952.

Mederios, B., D. L. Williamson, C. Hannay, and J. G. Olson (2012), Southeast Pacific stratocumulus in the Community Atmosphere Model. *J. Climate*, *25*, 6175–6192. DOI:10.1175/JCLI-D-11-00503.1

Moeng C.-H., P. P. Sullivan and B. Stevens (1999), Including radiative effects in an entrainment-rate formula for buoyancy driven PBLs. *J. Atmos. Sci.*, *56*, 1031–1049

Pincus, R. and S. A. Klein (2000), Unresolved spatial variability and microphysical process rates in large-scale models. *J. Geophys. Res.–Atmospheres*, 105, 27059–27065. doi:10.1029/2000JD900504.

Pincus, R., H. W. Barker, and J. J. Morcrette (2003), A fast, flexible, approximate technique for computing radiative transfer in inhomogeneous cloud fields. *J. Geophys. Res.–Atmospheres*, 108, 4376–4380. doi:10.1029/2002jd003322.

Randall, D. A., M. Khairoutdinov, A. Arakawa, and W. Grabowski (2003), Breaking the cloud-parameterization deadlock. *Bull. Amer. Meteor. Soc*., *84*, 1547–1564.

Randall D. A., W. H. Schubert (2004), Dreams of a stratocumulus sleeper. *In Atmospheric Turbulence and Mesoscale Meteorology, Scientific Research Inspired by Doug Lily*, edited by E. Fedorovich, R. Rotuno and B. Stevens, pp. 95-114, Cambridge University Press, Cambridge, UK.

Sandu, I., B. Stevens and R. Pincus (2010), On the transitions in marine boundary layer cloudiness, *Atmos. Chem. Phys.*, *10*, 2377–2391.

Skamarock, W. C., J. B. Klemp, J. Dudhia, D. O. Gill, D. M. Barker, M. G. Duda, W. Wang, and J. G. Powers (2008), A description of the advanced research WRF version 3, 113 pp., NCAR Technical Note, NCAR/TN-475+STR, National Center for Atmospheric Research, Boulder, CO.

Soden, B. J., and G. A. Vecchi (2011), The vertical distribution of cloud feedback in coupled ocean-atmosphere models, *Geophys. Res. Lett.*, *38*, L12704, doi:10.1029/2011GL047632.

Stevens, B., and coauthors (2001), Simulations of Trade Wind Cumuli under a Strong Inversion. *J. Atmos. Sci.*, *58*, 1870–1891.

Stevens, B., and coauthors (2005), Evaluation of Large-Eddy Simulations via Observations of Nocturnal Marine Stratocumulus. *Mon. Wea. Rev.*, 133,1443–1462.

©2014 American Geophysical Union. All rights reserved.

Stull R. B. (1988), *An Introduction to Boundary Layer Meteorology*. 666 pp., Kluwer Academic Publishers, Boston, MA.

Wang, H., and G. Feingold (2009a), Modeling mesoscale cellular structures and drizzle in marine stratocumulus. Part I: Impact of drizzle on the formation and evolution of open cells. *J. Atmos. Sci.*, *66*, 3237–3255.

Wang, H., and G. Feingold (2009b), Modeling mesoscale cellular structures and drizzle in marine stratocumulus. Part II: The Microphysics and Dynamics of the Boundary Region between Open and Closed Cells. *J. Atmos. Sci.*, *66*, 3257–3275.

Wang, H., W. C. Skamarock, and G. Feingold (2009), Evaluation of scalar advection schemes in the Advanced Research WRF model using large-eddy simulations of aerosol-cloud interactions. *Mon. Wea. Rev.*, *137*, 2547–2558.

Wood, R., and D. L. Hartmann (2006), Spatial Variability of liquid water path in marine boundary layer clouds: the importance of mesoscale cellular convection. *J. Climate*, *19*, 1748–1764.

Wood R., C. Bretherton, D. Leon, A. Clarke, P. Zuidema, G. Allen, and H. Coe (2011), An aircraft case study of the spatial transition from closed to open mesoscale cellular convection over the southeast Pacific. *Atmos. Chem. Phys.*, *11*, 2341–2370.

Wood R. (2012), Stratocumulus Clouds. *Mon. Wea. Rev.*, *140*, 2373–2423.

Wyant, M. C., C. S. Bretherton, H. A. Rand, and D. E. Stevens (1997), Numerical Simulations and a Conceptual Model of the Stratocumulus to Trade Cumulus Transition. *J. Atmos. Sci.*, *54*, 168–192.

Wyant, M. C. and Coauthors (2010), The PreVOCA Experiment: Modeling the lower troposphere in the Southeast Pacific. *Atmos. Chem. Phys.*, *10*, 4757–4774.

Xiao, H., C.-M. Wu, and C. R. Mechoso (2011), Buoyancy reversal, decoupling and the transition from stratocumulus-topped to trade-wind cumulus-topped marine boundary layer. *Climate Dyn.*, *37*, 971–984.

Xu, K.-M., and D. A. Randall (1995), Impact of interactive radiative transfer on the macroscopic behavior of cumulus ensembles. Part I: Radiation parameterization and sensitivity tests. *J. Atmos. Sci.*, *52*, 785–799.

Yamaguchi, T., and G. Feingold (2012), Technical note: Large-Eddy simulation of cloudy boundary layer with the Advanced Research WRF model, *J. Adv. Model. Earth Syst.*, *4*, M09003, doi:10.1029/2012MS000164.

Accepted Article

©2014 American Geophysical Union. All rights reserved.

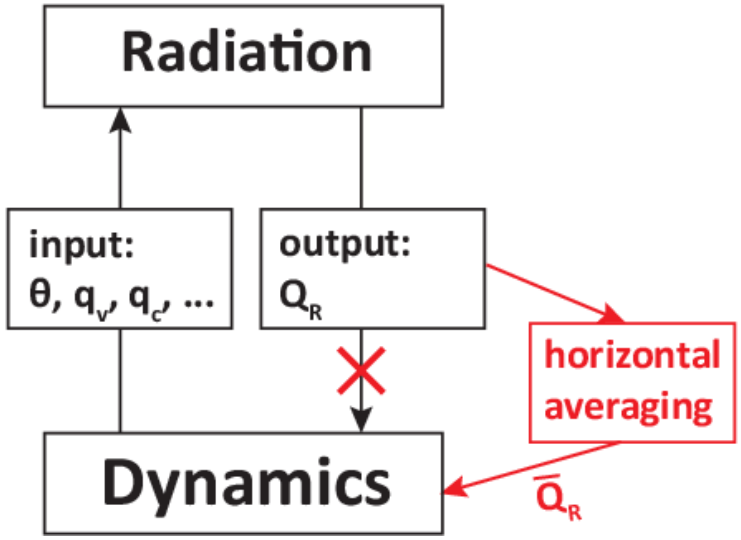

Figure 1

Accepted

©2014 American Geophysical Union. All rights reserved.

Accepted Article

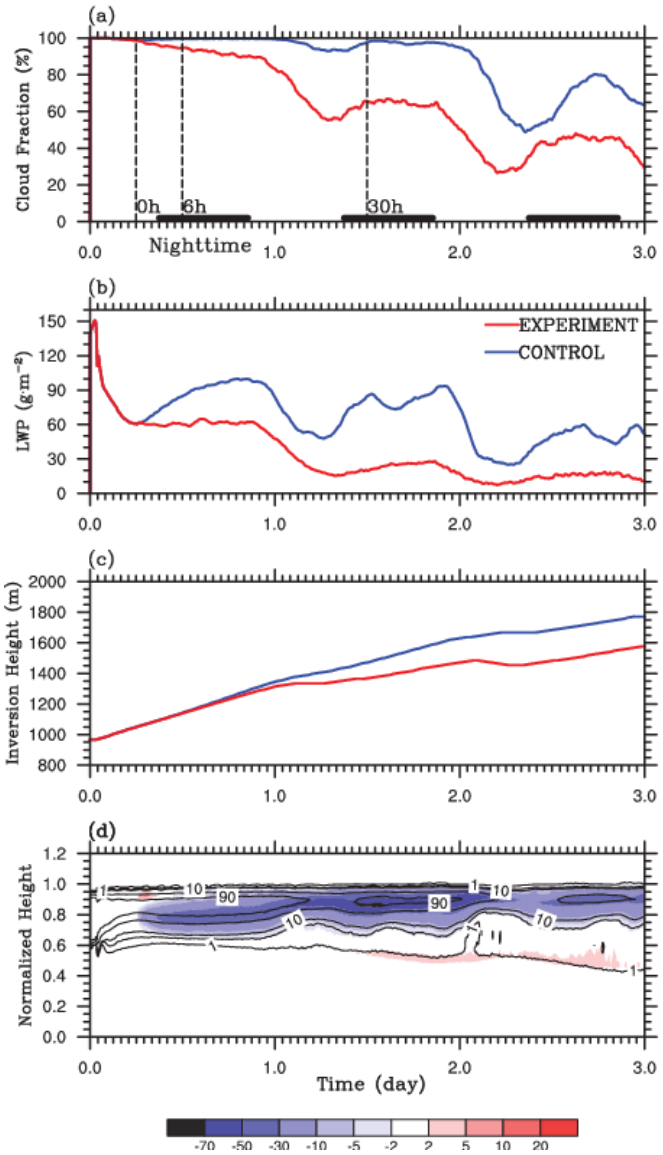

Figure 2

©2014 American Geophysical Union. All rights reserved.

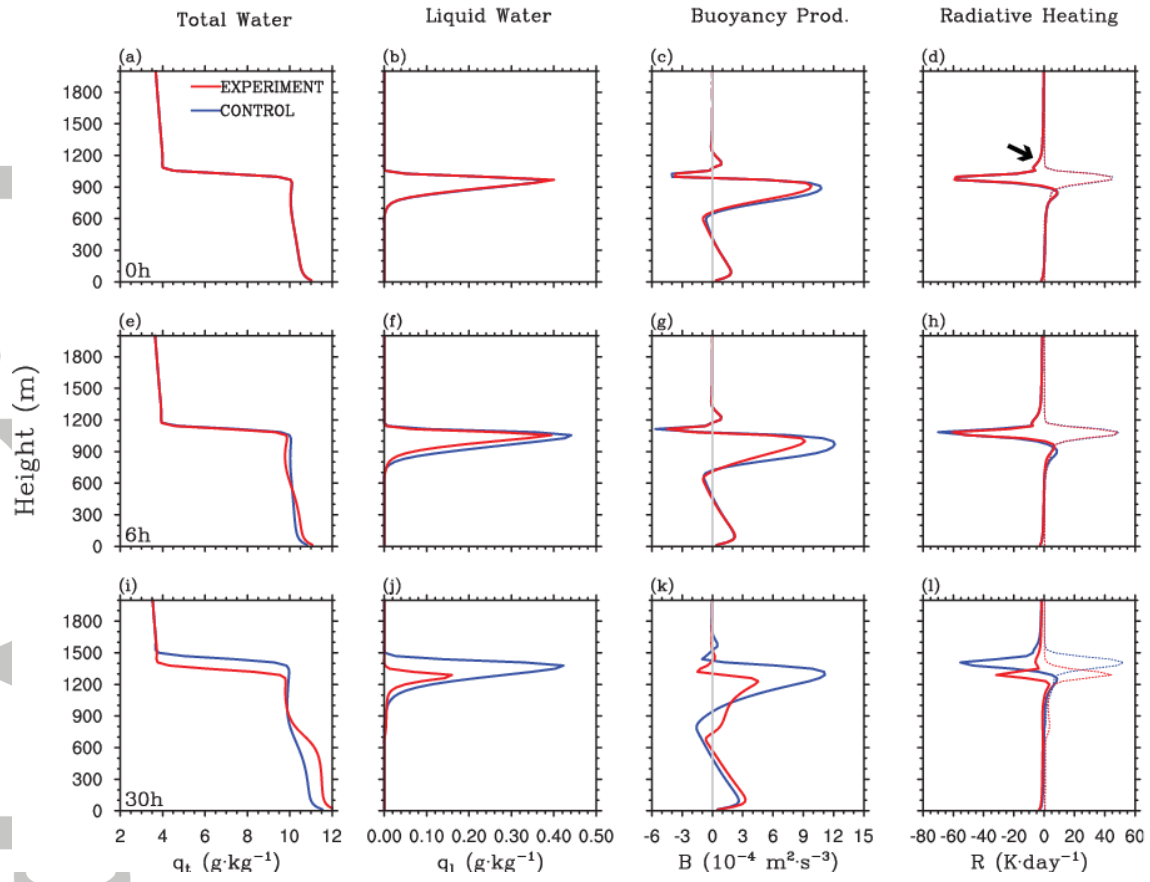

Figure 3

Accepted

©2014 American Geophysical Union. All rights reserved.

Accepted Article

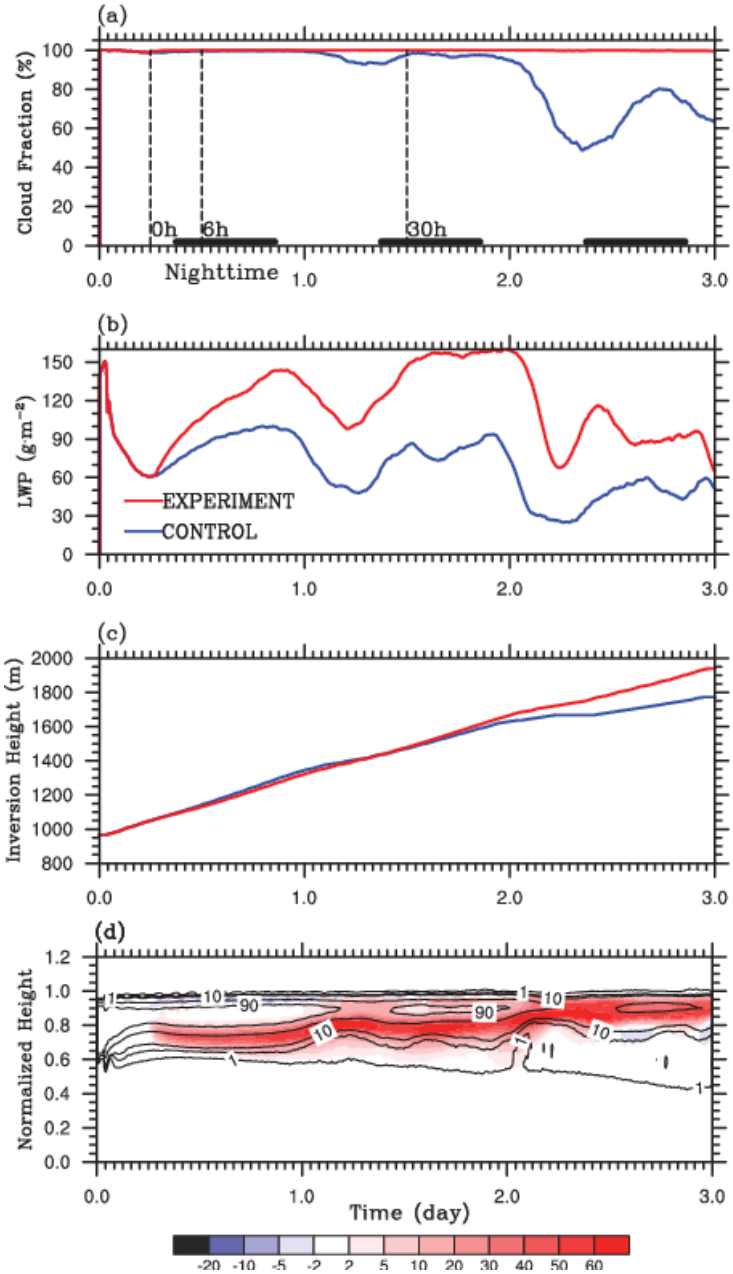

Figure 4

©2014 American Geophysical Union. All rights reserved.

Accepted Article

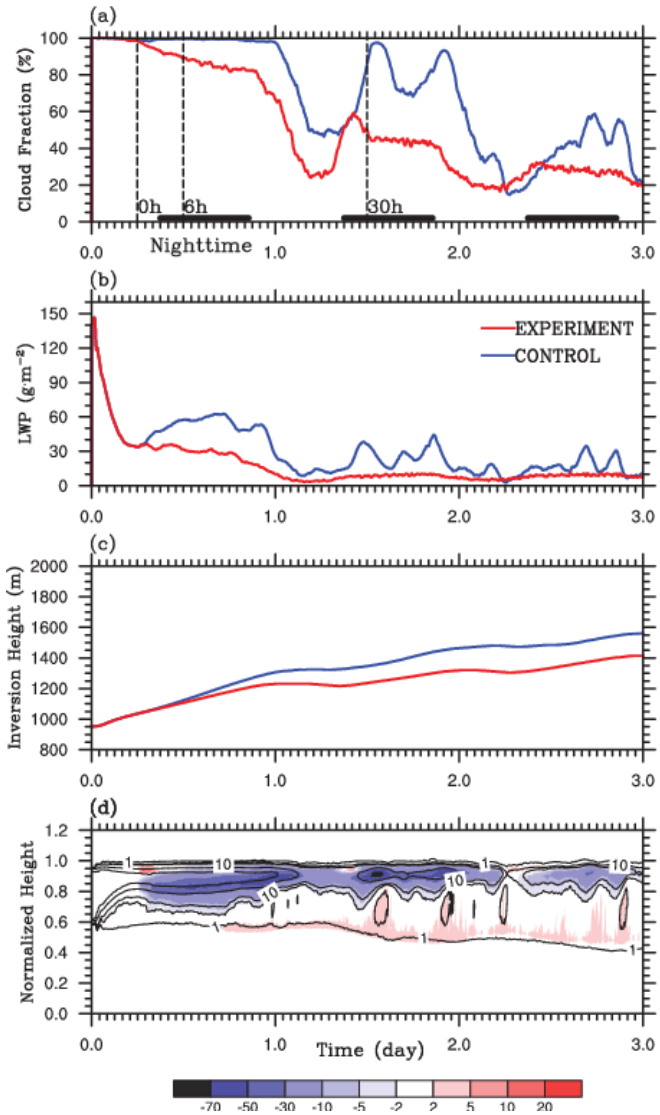

Figure 5

©2014 American Geophysical Union. All rights reserved.

Accepted Article

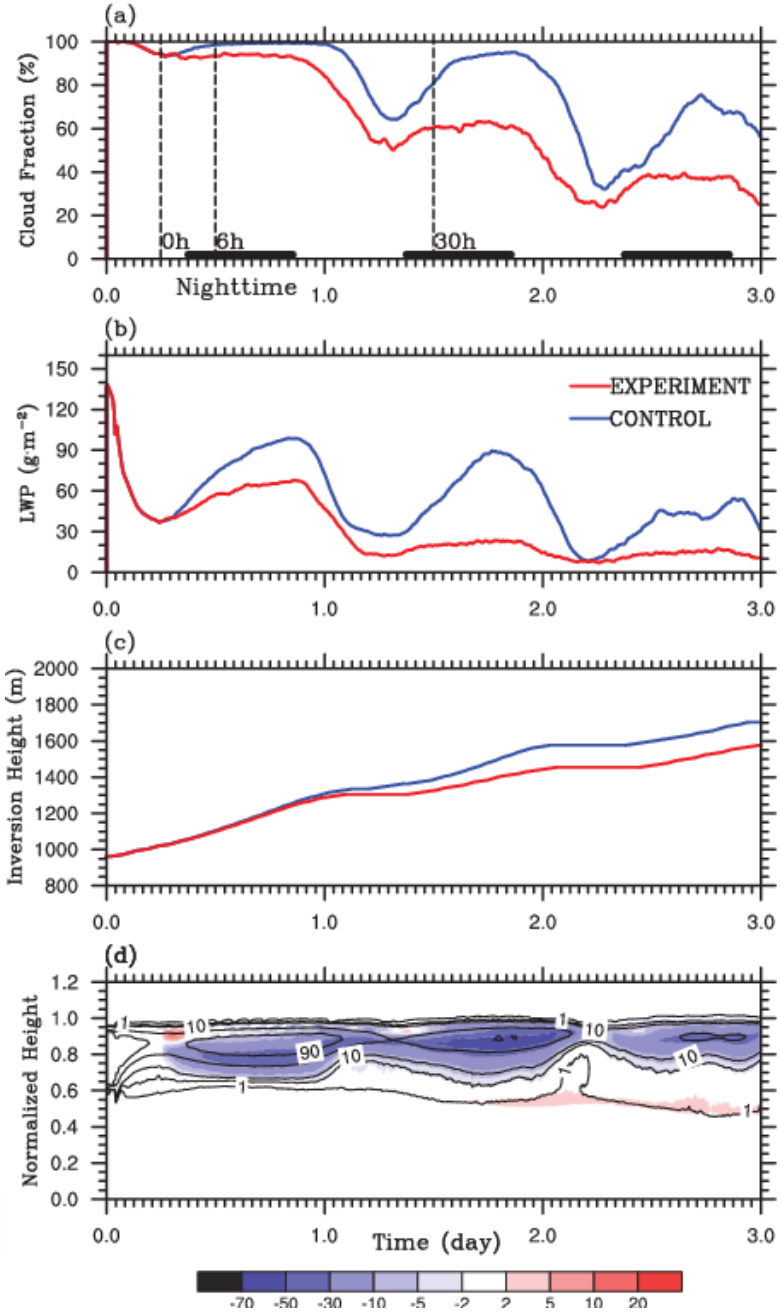

Figure 6

©2014 American Geophysical Union. All rights reserved.

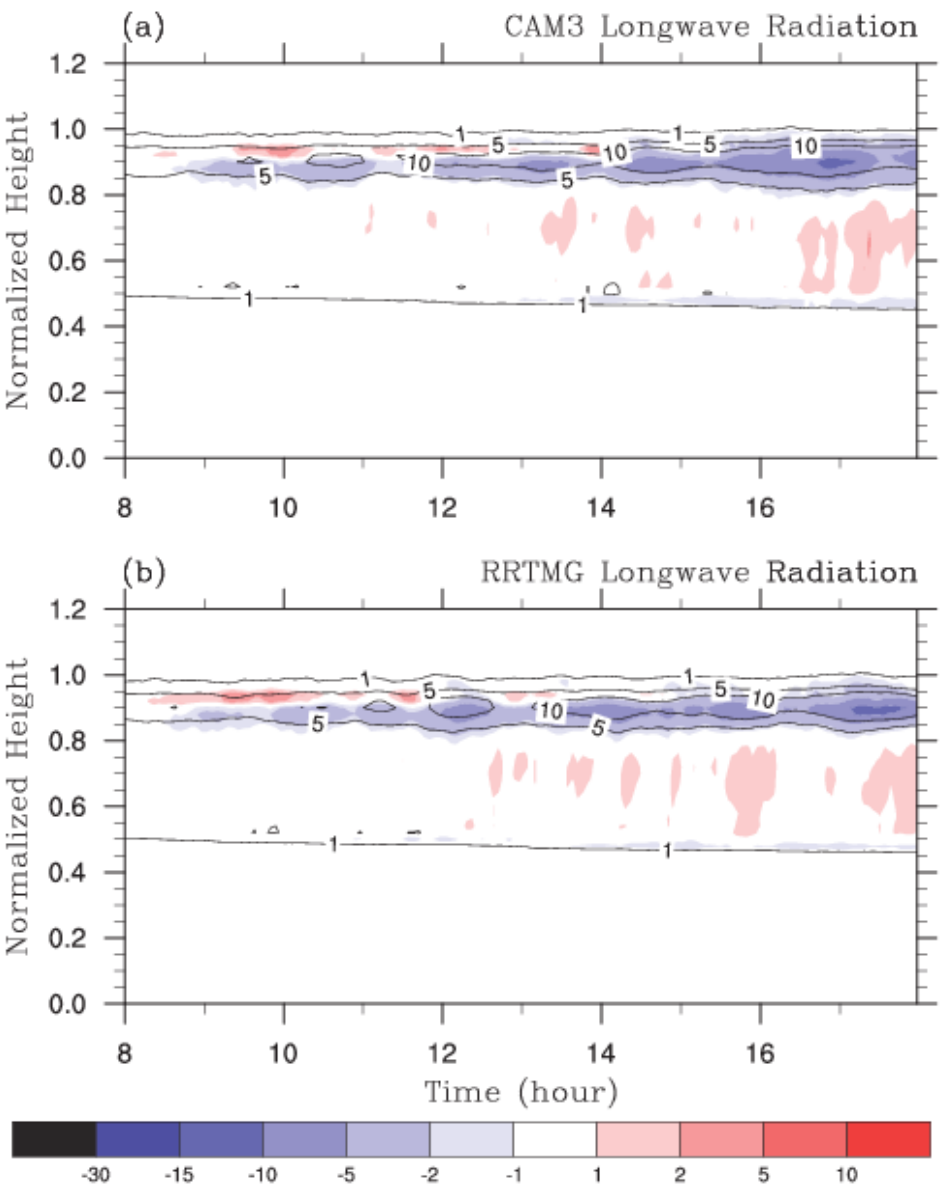

Figure 7

©2014 American Geophysical Union. All rights reserved.

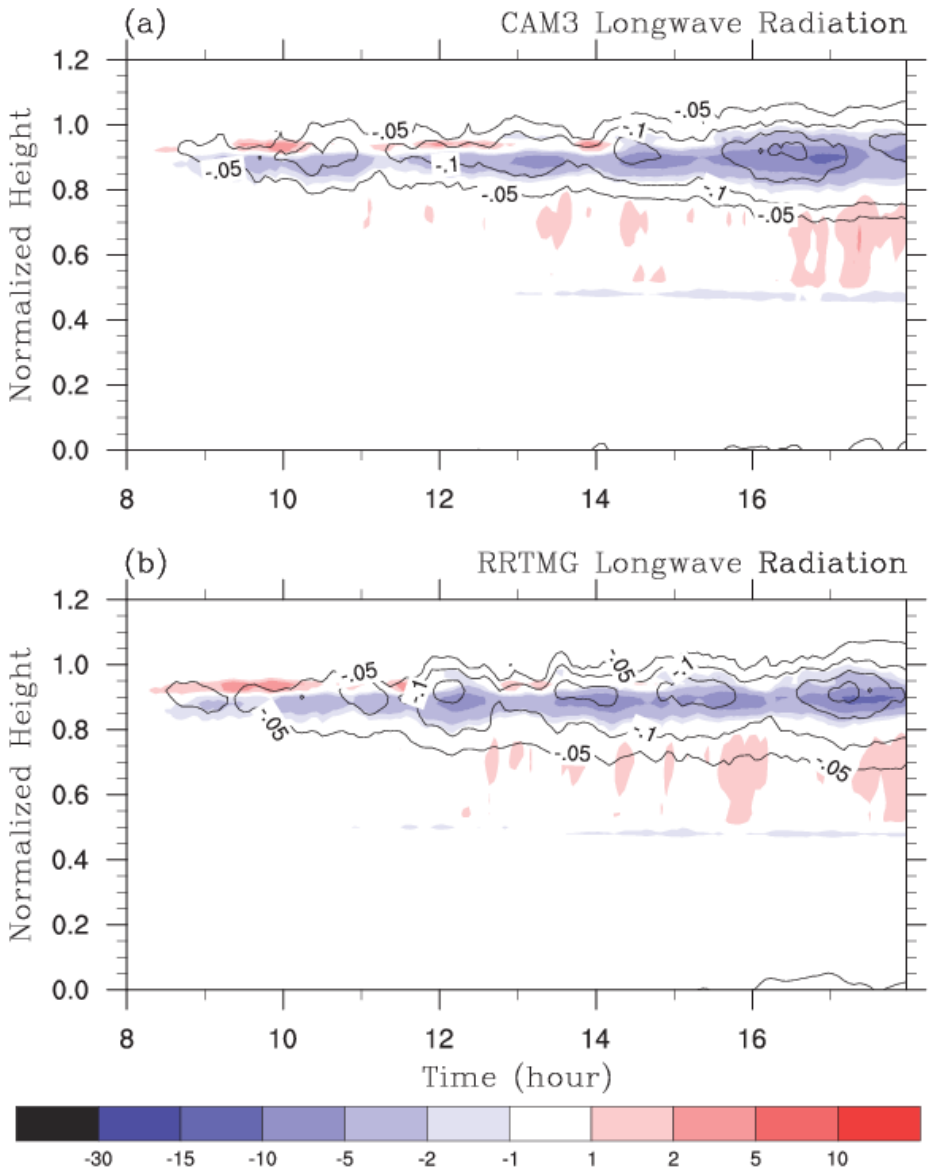

Figure 8

Accepted Article

©2014 American Geophysical Union. All rights reserved.

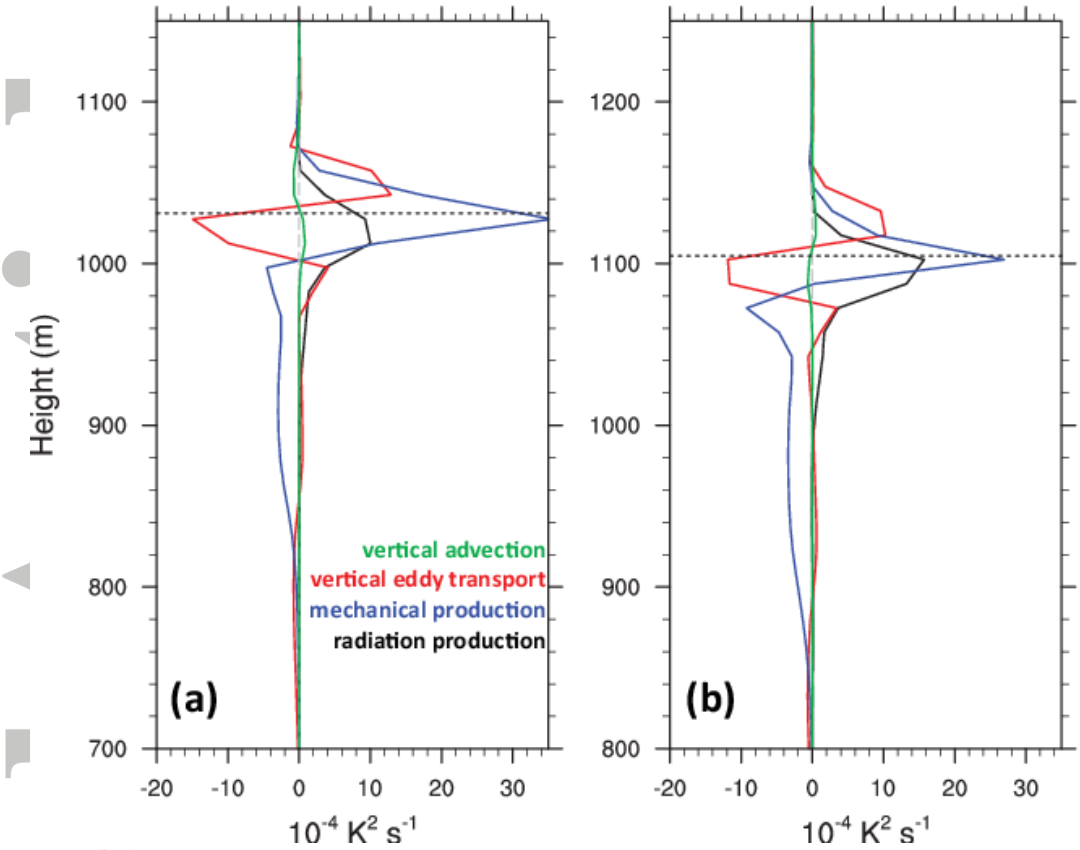

Figure 9

Accepted

©2014 American Geophysical Union. All rights reserved.